Available online at www.sciencedirect.com
ScienceDirect
International Journal of Heat and Mass Transfer 49 (2006) 5075–5080
International Journal of HEAT and MASS TRANSFER
www.elsevier.com/locate/ijhmt

Technical Note

On the role of heat and mass transport during the mutual annihilation of two premixed propane–air flames

Bhargav Ranganath, Tarek Echekki *

Department of Mechanical and Aerospace Engineering, North Carolina State University, Raleigh, NC 27695-7910, United States

Received 26 September 2005; received in revised form 18 May 2006
Available online 1 August 2006

Abstract

The unsteady process of mutual annihilation of two stoichiometric propane–air flames in one dimension is investigated numerically in the presence of preferential (the diffusion of heat relative to mass diffusion of species) and differential diffusion (the relative mass diffusions of species) effects. These effects are found during the early stages of mutual annihilation, corresponding to preheat layers' interactions, as well as during the merger of the reaction layers. The diffusive mobility of heat relative to the reactants results in the preheating of the reactants and associated increases in the rates of reactants' consumption. These rates are sustained during the merger of the reaction layers due to the relative mobility of the secondary fuels, especially H_2, which results in the build-up of radicals in the reaction zone prior to the completion of the mutual annihilation process. Preferential and differential diffusion effects also result in the formation of products of incomplete combustion at the end of this process.

1. Introduction

In turbulent flows, flames are continuously wrinkled and strained by the unsteady flow field. This wrinkling and straining process results in increased turbulent flame area, and accordingly in increased rate of volumetric heat release. Another competing process that becomes important with increased turbulence intensity is the increased rate of flame–flame interactions, which results in mutual flame annihilation and decreased flame area or flame shortening. While the statistics of this process are associated with turbulent transport, the actual process of flame–flame interactions is governed primarily by the coupling of molecular processes, reaction and diffusion. An understanding of the transient process of mutual annihilation can provide insight into improved models of turbulent combustion, as mutual annihilation is expected to be an important mechanism for flame shortening [1].

The present study is concerned with the evolution of the overall rate of reaction during the upstream interaction of propane–air flames in the presence of preferential (heat vs. mass) and differential (mass vs. mass) diffusion. Pertinent questions for turbulent combustion models are related to (1) the time scales associated with the interaction relative to turbulence and chemical time scales, (2) the role of mutual annihilation in the formation of products of incomplete combustion, and (3) the effects of preferential and differential diffusion on the mutual annihilation process.

The study is implemented numerically in 1D for two identical stoichiometric propane–air flames propagating into the space of reactants separating the two flames, and finally merging at the symmetry line. Similar transient simulations and analytical studies have been implemented for other flames in the past two decades [2–7]. Earlier studies also considered the interactions of premixed flames under steady conditions using the counterflow geometry [8–12]. However, transient studies provide direct assessments of the time scales of the mutual annihilation process. Although, the process of mutual annihilation occurs under curvature and straining conditions in turbulent flames, a

* Corresponding author. Tel.: +1 919 515 5238; fax: +1 919 515 7968.
E-mail address: techekk@eos.ncsu.edu (T. Echekki).

0017-9310/$ - see front matter © 2006 Elsevier Ltd. All rights reserved.
doi:10.1016/j.ijheatmasstransfer.2006.05.029

Nomenclature

h^s	sensible enthalpy	*Greek symbols*	
Δh_f°	species heat of formation	α	species index
Le	species Lewis number	δ_f	flame thermal thickness
S_C	flame consumption speed	$\dot{\omega}$	species reaction rate
S_L	laminar flame speed	ρ	density
t	time		
t_f	flame time	*Subscripts*	
T	temperature	b	burned gases state
x	distance along the flame normal	u	unburned gases state

simplified computation is used here to identify the coupling of molecular transport (for heat and mass) and chemistry in 1D. Preferential and differential diffusion effects are found to play important roles on the transient process of annihilation in methane–air and butane–air premixed flames [2–5]. These effects are found on the reactants' side [3,5] as well as within the reaction zone [2,4]. The recent study by Ranganath and Echekki [5] over a range of equivalence ratios from lean to rich hydrogen–air flames shows an overall consistent shift of chemistry during the initial stages of flame–flame interactions to leaner conditions due to the important differential diffusion of the fuel, H_2, in the reaction zone. Traditional theories based on the Lewis number of the deficient reactant, resulting in the 'flip' of the effective Lewis number of the mixture from lean to rich conditions, and vice-versa, are not applicable to the transient mutual annihilation process. The present study based on a less mobile fuel, propane, will confirm the contribution of a shift, in this case to rich mixture conditions, in equivalence ratio to the process of mutual flame annihilation. In comparison with the earlier study by Echekki et al. [4] based on methane we will attempt to identify the role of this shift on processes within the reaction zone. Methane has a comparable diffusive mobility to the oxidizer, O_2, and heat in contrast to H_2 and C_3H_8.

2. Numerical implementation

The computations are implemented in 1D using Sandia's S3D code. S3D is a compressible direct numerical simulation (DNS) flow code with a conservative formulation for the three components of the momentum, the density, the energy and the species mass densities. Transport properties are temperature and composition-dependent. The numerical scheme is based on an explicit eighth order finite difference scheme in space [13] and a fourth order accurate Range-Kutta temporal integration [14]. The non-reflecting boundary conditions are based on the NSCBC boundary conditions, which were originally developed by Poinsot and Lele [15] and modified for the present formulation by Mahalingam [16].

Temperature dependent properties are employed for the simulation using the formulation proposed by Smooke and Giovangigli [17] for the thermal conductivity, temperature dependent species specific heats using the CHEMKIN thermodynamic database [18]. A Lewis number formulation for species mass transport [17] is also adopted. It is based on assigning a constant Lewis number for different transport species relating its mass diffusivity to the thermal diffusivity. These Lewis numbers are evaluated using a least-square fit of the species diffusive fluxes for a range of temperatures between 500 and 2500 K using the PREMIX code [19]. The Lewis numbers of the species considered are C_3H_8(1.81), CO(1.07), CO_2(1.36), O_2(1.06), H_2O(0.79), H_2(0.29), OH(0.70), O(0.68), H(0.17), HO_2(1.06), CH_4(0.97), CH_3(0.96), CH(0.64), CH_2(0.94), CH_2O(1.24), HCO(1.23), C_2H_6(1.41), C_2H_5(1.39), C_2H_4(1.28), C_2H_3(1.28), C_2H_2(1.27), CH_3CHO(1.47), CH_3CO(1.46), CH_2CO(1.46), IC_3H_7(1.80), C_3H_6(1.79), H_2O_2(1.07) and N_2(1.02). Similarly, the Prandtl number relating the kinematic viscosity to the thermal diffusivity is set to a constant value of 0.708. Propane chemistry is based on the detailed propane mechanism M5 of Haworth et al. [20] with 28 species and 73 reversible elementary reactions. Initial profiles of the flames are obtained using the PREMIX code [19]; these profiles are allowed to reach steady-state in the S3D code prior to interactions between the two flames. The reactants' temperature is 300 K and the pressure is 1 atm. The domain length is 10.5 cm with 10,504 spatially-uniform grid points used.

The numerical results are presented in terms of global quantities and centerline values for key scalars. Global quantities include the consumption speed, S_C, which is the integrated reaction rate for the reactants or products normalized to yield units of speed. It corresponds exactly to the laminar 1D flame speed, S_L, at steady-state. Consumption speeds based on reactants or products are expressed as follows: $S_{C,\alpha} = \left[\int_{x=0}^{L} \dot{\omega}_\alpha \mathrm{d}x\right] / [\rho_u (Y_{\alpha,u} - Y_{\alpha,b})]$, where $\dot{\omega}_\alpha$ is the production rate for species α; Y's are the mass fractions; the subscripts u and b correspond to unburnt and burnt gas conditions; and ρ_u is the unburnt gas density. The consumption speed based on the heat release rate is expressed as follows: $S_{C,T} = \left[\int_{x=0}^{L} \left(-\sum_{\alpha=1}^{N} \Delta h_{f,\alpha}^\circ \dot{\omega}_\alpha\right) \mathrm{d}x\right] / [\rho_u (h_b^s - h_u^s)]$. Here, $\Delta h_{f,\alpha}^\circ h_u^s$, and h_b^s are the standard heat of formation of species α,

and the sensible enthalpies of the mixture at unburnt and burnt gas conditions, respectively.

Two additional scales based on the 1D steady flame are used to normalize our results. They are the thermal thickness, δ_f, which is defined as the ratio of the temperature difference across the flame to the maximum temperature gradient, $\delta_f = (T_b - T_u)/(dT/dx)_{max}$. The laminar flame speed, S_L, is also computed from steady laminar flame profiles. A characteristic flame time, t_f, may be derived from the ratio of the flame thickness to the laminar flame speed at steady-state conditions, $t_f = \delta_f/S_L$. The quantities, δ_f and t_f, are used to normalize length and time scales, respectively.

3. Results and discussion

To understand the mechanism of mutual annihilation in premixed propane–air flames, it is useful to briefly discuss the overall flame structure at steady-state. Fig. 1 a schematic of the overall structure of a stoichiometric premixed propane–air flame. The profiles are generated using steady-state solutions from DNS prior to the onset of mutual annihilation. The figure illustrates the typical asymptotic structure of hydrocarbon flames, which can be described in terms of distinct layers: (a) a preheat layer, (b) an inner or fuel consumption layer, (c) CO and H_2 oxidation layers, and post-flame layers. The vertical lines on the figure delineate the approximate limits of the layers. In the thin inner layer, the fuel and radicals are consumed to form secondary fuels, CO and H_2. The primary fuel, C_3H_8, does not reach beyond this layer; while, the oxidizer, O_2, continues to exist beyond it. In the oxidation layers CO and H_2 formed in the inner layer are oxidized to form CO_2 and H_2O. The profiles of H_2 and CO extend towards the product side, and similarly the temperature profiles approach slowly the adiabatic value in the post-flame. The overall structure of the propane–air flame is similar to that of methane-air flames [4], and is fundamentally different from the hydrogen flame [5]. The presence of a two-zone reaction structure and the formation of secondary fuels are found to play important roles during the intermediate stages of mutual annihilation in methane-air premixed flames [4], and are expected to play important roles in propane–air premixed flames as well. In methane–air flames, this role is characterized by the selective diffusion of the more mobile, H_2, relative to CO towards the reactants' side, which significantly enhances the rates of radical build-up and secondary fuels consumption prior to mutual annihilation. During the upstream interaction process between two premixed flames, preheat layers merge first, followed by the merger of the fuel consumption layers, and the CO and H_2 oxidation layers. Note in Fig. 1 the presence of a 'dip' or change of curvature in the profile of H_2O past the H_2 oxidation layer, which results from the presence of a thin layer of consumption for H_2O in the reaction zone.

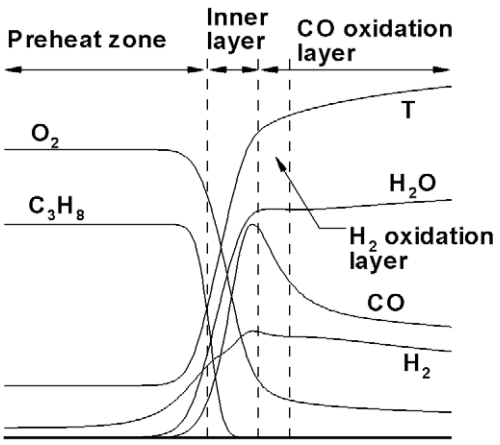

Fig. 1. Schematic of the overall structure of premixed propane–air flames.

3.1. Preheat layers' interactions

The stage of preheat layers' interactions corresponds to the merger of the preheat zone, which features primarily the coupling of convection and diffusion without chemistry or heat release. Fig. 2 shows the temporal evolution of the temperature and the reactants' mass fractions at the symmetry line between the flames. The species mass fractions are normalized by their initial values at the centerline prior to the onset of any interactions; the normalized temperature shown in the figure is expressed as $(T_b - T)/(T_b - T_u)$, where T_u and T_b are the steady-state flame unburnt and burnt gas temperatures, respectively. The onset of mergers of the diffusive and temperature layers is characterized by a departure from these initial values; while the order with which reactants and temperature layers merge depends on their rates of diffusion. In a manner consistent with the value of their Lewis numbers, which are both greater than one and therefore less diffusive, the reactants' diffusive layers lag the merger of the temperature layers. This merger

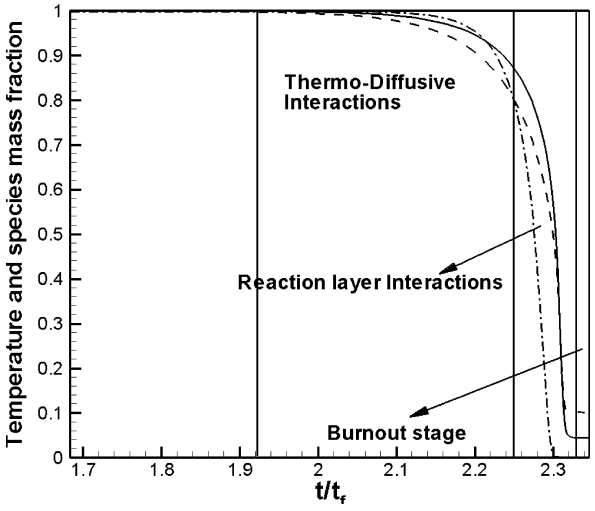

Fig. 2. Evolution of normalized propane and oxygen species mass fraction and temperature at the symmetry line during the various stages of mutual annihilation. T: (----), $Y_{C_3H_8}$: (–·–·–), Y_{O_2}: (—).

results in the preheating of the reactants. Also, consistent with the value of the O_2 Lewis number, the O_2 diffusion layer is the second layer to merge; while, propane, which has the highest Lewis number merges last. The order based on the value of the Lewis number is consistent with the order observed for H_2–air flames (see Fig. 2 in Ref. [5]); but, in contrast to these flames, it is the propane profile, owing to its lower diffusive mobility, that lags during the merger of the preheat layers. Therefore, the preheat layers, interactions, which occur in the absence of chemical reactions, are entirely governed by preferential diffusion (heat ahead of mass) and differential diffusion (oxygen ahead of propane) effects. Despite the fuel lag, the normalized value for C_3H_8 mass fraction decays afterward more rapidly due to the merger of the reaction layers and the depletion of C_3H_8 in the fuel consumption layer. This trend is seen in Fig. 2 and is shown by the rapid decay of the C_3H_8 mass fraction. This decay is accompanied by the formation of the secondary fuels CO and H_2 as discussed earlier. The higher diffusive mobility of O_2 compared to C_3H_8 during the preheat layers' interactions result in an initial shift of the effective equivalence ratio at the centerline to lean conditions in the reaction zone, followed by a shift to richer conditions towards the end of the mutual annihilation process. These shifts, although not explicitly shown here, and which are associated with differential diffusion play key roles in the generation of products of incomplete combustion or dissociation products at the end of the process.

The vertical lines in the figure delimit the approximate times corresponding to the onset of the various stages of mutual annihilation. The time period associated with preheat layers' interactions is relatively longer than the corresponding period for the reaction layers' interactions. The burnout stage lasts the longest and past the period shown in the figure. The preheat layers' interactions lasts approximately 0.3 t_f; while, the reaction layers' interactions last less than 10% of t_f. These fractions illustrate the rapid process of mutual annihilation. While these time scales appear to be consistent with the relative time scales of diffusion and reaction, it is evident from these scales that an accelerated merger of the preheat and the reaction layers is occurring during the mutual annihilation process. Although not shown here, the accelerated merger of the preheat layers is primarily a result of changes in the balance of reaction and diffusion in the reaction zone [4]. As discussed below, the acceleration of the merger of the reaction layers is governed by a rapid increase in the rates of consumption of the primary (C_3H_8) and secondary (CO and H_2) fuels during the reaction layers' interactions.

3.2. Reactions layers' interactions

Fig. 3 shows the evolution of the consumption speeds for the reactants, C_3H_8 and O_2, the products, H_2O and CO_2, and the temperature-related consumption speed, associated with the heat release rate. These are the integrated reaction rates over the entire domain, and are normalized by the corresponding value at steady-state. The figure shows that the consumption speed increases at the initial stages of the reaction layers' interactions for both reactants and products, albeit at different rates. Propane exhibits an earlier decay associated with the complete consumption of the fuel in the fuel consumption layer; beyond the merger of this layer, O_2 continues to be consumed in the H_2 and CO oxidation layers. The peaks of H_2O and CO_2 follow. The reaction layers' interactions process results in an increase of the O_2 consumption speeds and consumption speed associated with heat release by approximately a factor of 2, and approximately 1.7 times for H_2O and CO_2; while, the consumption speed of C_3H_8 increases by a factor of only 10%, approximately. The moderate increase in C_3H_8 consumption speed can be attributed primarily to the preheating effect resulting from the merger of the temperature layers first. The increases associated with the heat release rate, O_2 consumption and products consumption is associated with the CO and H_2 oxidation layers, and can be attributed mainly to the secondary fuels, CO and H_2. The consequences of these increases are also closely related to an increase in the radical pool and the peak temperature in the reaction zone. Fig. 3 also shows that towards the completion of the merger of the reaction layers, the consumption speed associated with H_2O decreases below zero prior to recovering a positive value. The negative value is associated with the contribution of a consumption layer for H_2O in the absence of the dominant contribution of the production layers that has merged. Evidence of this consumption layer can also be seen in the profiles of H_2O at steady-state (Fig. 1).

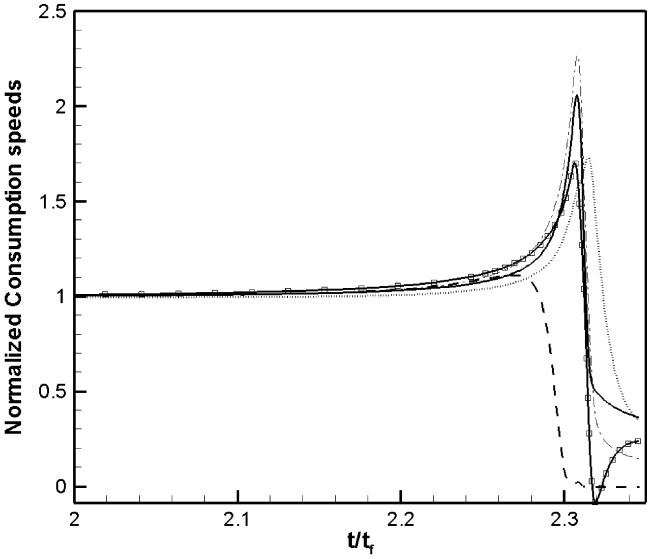

Fig. 3. Evolution of normalized temperature related consumption speed and consumption speeds for C_3H_8, O_2, CO_2 and H_2O. Heat Release Rate: (—), C_3H_8: (----); O_2: (–·–·–); CO_2: (. . .. . .); H_2O: (–□–□–).

The reaction layers' interactions start with the merger of the thin fuel consumption layer, which results in the emer-

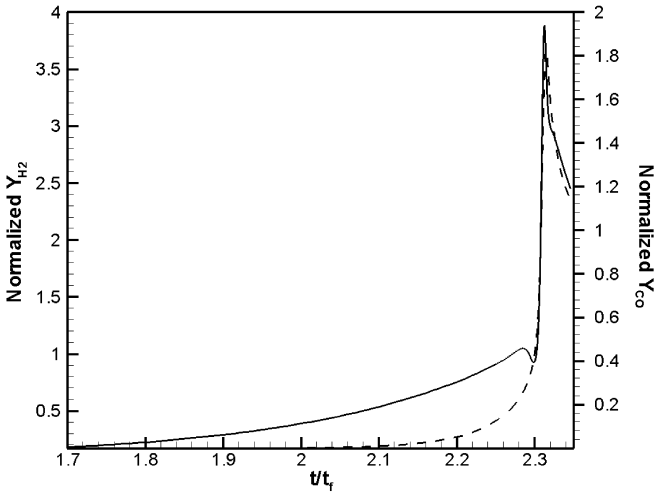

Fig. 4. Evolution of normalized H_2 and CO species mass fractions at the symmetry line. H_2: (—); CO: (----).

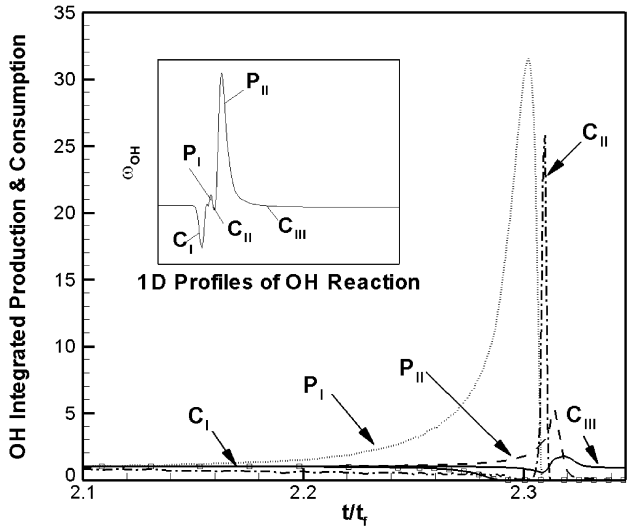

Fig. 5. Evolution of the normalized integrated production and consumption rates for species OH. Consumption layer I: (–□–); Production layer I: (……); Consumption layer II: (–·–·–); Production layer II: (----); Consumption layer III: (—).

gence of H_2 ($Le = 0.29$) and CO ($Le = 1.07$) as the primary fuels during the later stages of the interactions. Because these two fuels have different mass diffusive properties, with respect to each others, and heat and the oxidizer, important differential diffusion effects are observed.

Fig. 4 shows the temporal evolution of the normalized species mass fractions of H_2 and CO at the symmetry line. The values are normalized by the peak mass fractions corresponding to the steady-state flame. The figure shows that both species mass fractions increase significantly beyond the peak value of the steady-flame, indicating that this increase is not only due to the presence of chemistry, but also to important couplings of differential diffusion and chemistry effects at the centerline. The different trends of H_2 and CO are also illustrated by the different degrees of 'leakages' of these two species into the preheat layers as shown by steady-state profiles. The basic consequence of the H_2 higher mobility is the accumulation of H_2 concentration at the symmetry line during intermediate stages of the reaction layers' interactions. The figure also shows excess CO and H_2 remaining at the symmetry line towards the end of burnout stage; the excess is associated with the depletion of the oxidizer, O_2. Once radicals are depleted at the final stages of mutual annihilation, these unburnt reactants also constitute products of incomplete combustion.

Fig. 5 shows the temporal evolution of the spatial integrals of the reaction rates for each consumption and production layer evaluated individually for the OH radical; the behavior of this radical is consistent with that of H and O as well. The integrated reaction rates are normalized by their steady-state values prior to the onset of any interactions. The reaction zone structure for OH production and consumption is relatively complex, and is made up of two production layers and three consumption layers. The sequence of the reaction layers with respect to their proximity to the reactants is as follows: consumption layer I, production layer I, consumption layer II, production layer II, and finally consumption layer III. The merger of the first production and consumption layers result in steady decays of their corresponding integrated values relative to the steady-state values. Although, more details can be discussed in the figure, we point out two main observations. During the merger of the inner layer, which is completed at approximately $t/t_f = 2.3$ (as shown in Fig. 2), consumption layer I continues to decrease, while production layer I steadily increases. This decrease in OH consumption is associated with the depletion of available fuel, C_3H_8, during the merger of the inner layer; while, the production is associated with the same mechanism, which leaves more radicals unconsumed by the fuel, and an enhancement of the chain-branching process. After the merger of the inner layer, the maximum value of the integrated reaction in production layer I increases to values above thirty times the steady value. This represents a continuation of the above-described process; however, this time, this process is accelerated by the availability of excess H_2 in the reaction zone (as seen in Fig. 4). OH production and consumption layers towards the products' side (consumption and production II, and consumption III) experience similar trends behind the peak in production layer I. Although not shown here, rates of production and consumption of H_2 and CO are significantly increased at this time due to the increased radical pool. These dramatic increases contribute to the accelerated rates of merger of the reaction zones during the mutual annihilation process of propane–air flames.

4. Conclusions

The main findings of the present study may be summarized as follows:

- The process of mutual annihilation resulting from upstream interaction in propane–air flames occurs over relatively short time scales compared to characteristic flame times.
- The process is further accelerated by preferential and differential diffusion. During the merger of preheat layers, the preferential diffusion of heat results in the preheat of the reactants, while the differential diffusion of the reactants results in shifts in the equivalence ratios in the reaction zone. During the merger of the reaction layers, the differential diffusion of the secondary fuel, H_2, into the symmetry plane results in the build-up of radicals, and subsequent acceleration of the consumption and production rates of secondary fuels and products.
- Differential diffusion also results in the incomplete burning of the secondary fuels, H_2 and CO.

Acknowledgement

This work was supported by the National Science Foundation, Chemical and Transport Systems Program. We thank Professor Dan Hawoth of Penn State University for providing the propane mechanism.

References

[1] S.M. Candel, D. Veynante, F. Lacas, E. Maistret, N. Darabiha, T. Poinsot, The coherent flame model: application and recent extension, in: B. Larrouturou (Ed.), Recent Advances in Combustion Modelling, World Scientific, Singapore, 1990, pp. 19–64.
[2] C.L. Chen, S.H. Sohrab, Upstream interactions between planar symmetrical laminar methane premixed flames, Combust. Flame 101 (1995) 360–370.
[3] W.J. Sheu, M.C. Lin, S.A. Yang, Upstream interactions between premixed flames, Combust. Sci. Tech. 111 (1995) 1–17.
[4] T. Echekki, J.H. Chen, I.R. Gran I., The mechanism of mutual annihilation of stoichiometric premixed methane–air flames, Proc. Combust. Inst. 26 (1996) 855–863.
[5] B. Ranganath, T. Echekki, Effects of preferential and differential diffusion on the mutual annihilation of two premixed hydrogen–air flames, Combust. Theo. Model. 9 (2005) 659–672.
[6] I.S. Wichman, R. Vance, A study of one-dimensional premixed flame annihilation, Combust. Flame 110 (1997) 508–523.
[7] Z.B. Lu, S. Ghosal, A similarity solution describing the collision of two planar premixed flames, Combust. Theo. Model. 7 (2003) 645–652.
[8] H. Tsuji, I. Yamaoka, Structure and extinction of near-limit flames in a stagnation flow, Proc. Combust. Inst. 19 (1982) 1533–1540.
[9] S.H. Sohrab, Z.Y. Ye, C.K. Law, An experimental investigation on flame interaction and the existence of negative flame speeds, Proc. Combust. Inst. 20 (1985) 1957–1965.
[10] P.A. Libby, F.A. Williams, Strained premixed laminar flames with 2 reaction zones, Combust. Sci. Tech. 37 (1984) 221–252.
[11] S.H. Sohrab, Z.Y. Ye, C.K. Law, Theory of interactive combustion of counterflow premixed flames, Combust. Sci. Tech. 45 (1986) 27–45.
[12] S.H. Chung, J.S. Kim, C.K. Law, Extinction of interacting premixed flames: theory and experimental comparisons, Proc. Combust. Inst. 21 (1988) 1845–1851.
[13] C.K. Kennedy, M.H. Carpenter, Several new numerical methods for compressible shear-layer simulations, Appl. Num. Math. 14 (1994) 397–433.
[14] C.K. Kennedy, M.H. Carpenter, R.M. Lewis, Low-storage, explicit Runge–Kutta schemes for the compressible Navier–Stokes equations, Appl. Num. Math 35 (2000) 177–219.
[15] T. Poinsot, S.J. Lele, Boundary conditions for direct simulations of compressible viscous flows, J. Comput. Phys. 101 (1992) 104–129.
[16] S. Mahalingam, Private Communications, 1993.
[17] M.D. Smooke, V. Giovangigli, in: M.D. Smooke (Ed.), Lecture Notes in Physics 384, Springer-Verlag, New York, 1991, Chap. 1.
[18] R.J. Kee, F.M. Rupley, J.A. Miller, The Chemkin thermodynamic data base, SAND87-8215, Sandia National Laboratories, 1987.
[19] R.J. Kee, J.F. Grcar, M.D. Smooke, J.A. Miller, A Fortran program for modeling steady laminar one-dimensional premixed flames, SAND85-8240, Sandia National Laboratories, 1985.
[20] D.C. Haworth, R.J. Blint, B. Cuenot, T.J. Poinsot, Numerical simulation of turbulent propane–air combustion with nonhomogeneous reactants, Combust. Flame 121 (2000) 395–417.